Space mapping filter design and tuning techniques

J. C. Melgarejo[1], J. Ossorio[1], A. A. San-Blas[2], M. Guglielmi[1] and V. E. Boria[1]

[1]Universitat Politècnica de València, Camino de Vera, Valencia, Spain and [2]Av. Universitat d'Elx, Elche, Spain

Abstract

A common strategy to reduce the cost of a filter is to use a manufacturing technique with an intermediate accuracy and use tuning elements to compensate for the manufacturing errors. However, including tuning elements in the final EM simulations, and tuning the filters after manufacturing, can be quite challenging. In this context, therefore, we review in this paper two powerful filter design procedures based on Aggressive Space Mapping (ASM), and two semi-automatic tuning techniques. As a validation, we describe in detail the design and tuning of two types of filters that are commonly used for both space and ground applications, namely, a six-pole inductive filter in rectangular waveguide, and a more complex five-pole filter based on dual-mode resonators.

Introduction

The increasing demand for more advanced communication systems with wider channel bandwidths has recently motivated space companies to explore the use of higher frequency bands (such as Ku, K, and Ka) that can easily accommodate higher transmission rates [1].

However, the use of higher frequency bands poses a series of mechanical problems when manufacturing waveguide devices in general, and in particular with respect to waveguide filters. It is, in fact, well known that as the frequency increases, the wavelength decreases, and the physical size of the components becomes smaller. As a result, the devices become much more sensitive to errors in the manufacturing processes. A practical solution to compensate for the errors without greatly increasing the cost of the filters is to use a manufacturing technique with an intermediate accuracy, like milling, and to use tuning elements to recover the desired response.

This, in turn, introduces a complication, namely, the manual tuning of the filter after manufacturing. Adjusting manually the tuning elements of a filter is, in fact, a complex and time-consuming task that, in general, requires extensive tuning experience [2].

Furthermore, the use of milling and tuning elements introduces two more challenges. The first one is that using milling we inevitably introduce rounded corners in the hardware. The rounded corners must then be included in the electromagnetic (EM) simulations, and this can significantly increase the required computational effort. The second challenge is that the presence of tuning elements must also be taken into account, and this can increase even further the computational effort. In this context, we must also remember that most microwave filter structures are currently designed using optimization procedures that normally require a large number of repeated EM simulations. A small increase in the time required for the EM simulation can therefore have a very significant negative effect.

Fortunately, however, the field of EM-based optimization of complex structures has recently made very significant progress due to the introduction of Space Mapping (SM) [3] and Aggressive Space Mapping (ASM) [4–15]. SM uses two simulation spaces, or *models*. A fast and low accuracy model, the so-called *coarse* model, and a precise but time-consuming model, the so-called *fine* model. The basic idea behind SM (and ASM) is that most simulations are performed using the coarse model, and the fine model is only used to verify the performance of the device in the various stages of the optimization process.

Significant effort has also been devoted in the past to the development of advanced CAD filter tuning procedures. Examples are the use of fuzzy logic [16], and machine learning [17, 18], to cite a few. A significant recent development in this area has been the use of SM to develop very efficient and effective CAD tuning procedures [19, 20].

In this context, therefore, the objective of this contribution is to provide, in a single paper, detailed information about the use of advanced SM techniques for both filter design and tuning. In addition to theory, we discuss in detail the design and tuning process of two types of filters that are commonly used for both ground and for space applications, namely, an inductive rectangular waveguide filter, and a more complex dual-mode filter.

The remainder of the paper is organized as follows. In Section "Design techniques", we discuss in detail the design of the filters. In Section "Tuning techniques", we show the most

adequate tuning strategy to be used in each case. Finally, in Section "Conclusions", we conclude the paper with a summary of the results that we have obtained.

Design techniques

In this section, we show how to design an inductive filter in rectangular waveguide and a compact filter based on dual-mode resonators. For each case, we compare the performances of two ASM-based design procedures [11, 12].

Inductive filter

Inductive filters in rectangular waveguide are very commonly used for both ground and space applications. In this section, we describe the design procedure for the six-pole filter shown in Fig. 1 (top). The center frequency of the filter is 11 GHz, and the bandwidth is 500 MHz. In order to reduce production costs, the filter will be manufactured using H-plane milling with an intermediate accuracy, namely, between 50 and 100 μm. As a consequence, all concave corners will be rounded in the final hardware. The filter will also use tuning elements (with 1.6 mm radius) both in the cavities and in the coupling irises. In the design process, all the tuners will be set to a penetration of 2 mm. This value is chosen to allow for future bidirectional adjustments.

The design process starts with a distributed model based on transmission lines and inverters that produce the desired Chebyshev response, i.e. the target of our design. Once we have obtained the distributed model, we can apply the design procedure described in [21] in order to obtain the initial *ideal* waveguide model of the filter shown in Fig. 1 (bottom). If we use a Multimode Equivalent Network (MEN) simulator, such as FEST3D, with a low accuracy setting, the EM analysis will require a very short time, and we will be able to rapidly optimize the structure and obtain the desired target performance.

At this point, the most time-consuming part of the design begins: we need to include all non-ideal elements, namely, the tuning elements and the rounded corners, and optimize the final filter structure with a high accuracy simulator. We could decide, for instance, to use FEST3D in a high accuracy setting, or a finite-element method solver, like CST or HFSS. In any case, the time required to carry out this step will be significant. We will now show how ASM can be very effectively exploited to reduce very significantly the computational effort.

OS-ASM

As already mentioned, the idea behind any SM-based optimization method is to use two simulations models: a fast model, called the coarse model (or *space*), and a precise but time-consuming model, the fine model. The key assumption behind SM (and ASM) is that the two spaces are related by the following linear equation (or *mapping*):

$$\mathbf{x_f} = \mathbf{B} \cdot \mathbf{x_c} + \mathbf{C} \qquad (1)$$

where $\mathbf{x_f}$ and $\mathbf{x_c}$ are the dimensions of the fine (Fig. 1, top) and coarse (Fig. 1, bottom) models, respectively. Furthermore, if we call the performances in the two spaces $R_f(\mathbf{x_f})$ and $R_c(\mathbf{x_c})$, respectively, we can write:

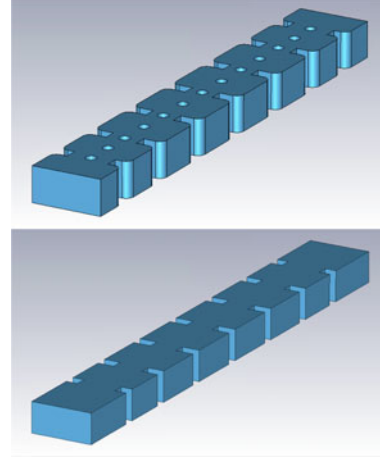$$R_f(\mathbf{x_f}) = R_c(\mathbf{x_c}) \qquad (2)$$

Fig. 1. Inductive six-pole filter. Top: Fine model of the filter. Bottom: *Ideal* coarse model of the filter.

to state that we have the same identical response in the two spaces. This is, in fact the objective that we want to obtain, namely, a set of dimensions for a filter structure that when manufactured and measured gives the same exact response of our ideal filter.

The matrix $\mathbf{B}$ in (1) is the so-called mapping matrix between the two spaces, and $\mathbf{C}$ is a vector of constants. In the traditional ASM optimization procedure [4], $\mathbf{B}$ is first set to be equal to the identity matrix, and it is then *updated* after each iteration. At the end of the process, when we reach the condition stated in (2), we can say that the coarse and fine models are perfectly *aligned*, and the matrix $\mathbf{B}$ correctly maps both spaces. Furthermore, it can be demonstrated mathematically that this optimization process will converge in a number of iterations that is proportional to the number of variables involved in the process.

Furthermore, recent research on ASM [11] indicates that the matrix $\mathbf{B}$ has the following, very important property. If the geometry of the coarse model is exactly identical to the geometry of the fine model, and the only difference between the two spaces is the accuracy of the computations, the correct value of $\mathbf{B}$ is, in fact, the identity matrix, and the ASM optimization process converges *in just one step*. This is, indeed, the origin for the name One-Step ASM (OS-ASM) in [11].

In the case we are discussing now, however, the coarse and the fine models are not exactly identical, as we can see in Fig. 1. The OS-ASM optimization process will therefore not be able to converge in one single step. However, the results obtained in [11] indicate that, using the identity matrix as the mapping matrix will result in a faster convergence with respect to the original ASM procedure described in [4].

The OS-ASM design process of the six-pole filter under examination is detailed next.

(i) Obtain first the (optimum) dimensions of the coarse model of the filter using, for instance, the procedure described in [21].

(ii) Set the initial dimensions of the fine model to the optimum dimensions of the coarse model (i.e. $\mathbf{x_{fl}} = \mathbf{x_{copt}}$), and add all non-ideal elements. Next carry out the first high accuracy simulation. Naturally, the electrical response that we obtain ($R_f(\mathbf{x_{fl}})$) will be (strongly) detuned ($R_f(\mathbf{x_{fl}}) \neq R_c(\mathbf{x_{copt}})$).

Table 1. Evolution of the design parameters for the inductive six-pole filter in the OS-ASM process. The design variables are the widths of the apertures (their thickness is fixed to 3.5 mm) and the lengths of the resonators (their heights and widths are set to 9.525 and 19.95 mm). All dimensions are in mm

Parameter	Coarse Optimum	Fine				
		Iter. 0	Iter. 1	Iter. 2	Iter. 3	Iter. 4
i_1	6434FC 12.1369	6434FC 12.1369	11.9197	11.9526	11.9587	11.9289
l_1	6434FC 13.8491	6434FC 13.8491	13.5647	13.4252	13.4502	13.4960
i_2	6434FC 9.0745	6434FC 9.0745	8.9056	8.8446	8.9010	8.8816
l_2	6434FC 16.2220	6434FC 16.2220	15.8992	15.8932	15.8904	15.8452
i_3	6434FC 8.3179	6434FC 8.3179	8.1048	8.1183	8.0983	8.1331
l_3	6434FC 16.6566	6434FC 16.6566	16.3419	16.3229	16.3354	16.3272
i_4	6434FC 8.1931	6434FC 8.1931	8.0575	7.9744	7.9603	7.9995

(iii) Optimize one instance of the coarse model until the performance of the fine model is matched, that is $R_c(\mathbf{x_{c1}}) = R_f(\mathbf{x_{f1}})$.

(iv) The next step is to compute the following differences:

$$\Delta = \mathbf{x_{copt}} - \mathbf{x_{c1}} \tag{3}$$

(v) We then update the dimensions of the fine model using the following equation:

$$\mathbf{x_{f2}} = \mathbf{x_{f1}} - \Delta \tag{4}$$

and perform another fine model simulation.

(vi) At this point we have completed the first iteration. We can therefore evaluate the error between $R_f(\mathbf{x_{f2}})$ and the desired target response. If the error is acceptable, we have concluded our process. If it is not acceptable, we go back to the second step and perform another iteration using $\mathbf{x_{f2}}$ as a starting point.

Applying to our filter the procedure just described, the coarse and fine models give essentially the same response after only four iterations. Table 1 shows the evolution of the design parameters in the OS-ASM process.

Efficient ASM

A more efficient alternative is to use the approach described in [12]. This second method combines the segmentation strategy of [21] with the power of OS-ASM. Instead of trying to optimize all design parameters simultaneously, the filter is designed step by step as follows:

(i) Obtain first the (optimum) dimensions of the low accuracy model of the filter.

(ii) Simulate the first three elements of the low accuracy model, namely, the first cavity with the relative input and output irises (see Fig. 2(a)). This model provides the first target that the equivalent high accuracy model of the filter (see Fig. 2(b)) must match.

(iii) Perform an OS-ASM iteration with the reduced coarse and fine models (shown in Figs 2(a) and 2(b)) until the reduced fine model produces the desired target response. Note that since we are dealing with reduced models, there are only three parameters to optimize, namely, the widths of the first two apertures and the length of the first cavity.

(iv) Add the next cavity of the filter to the reduced coarse model and obtain the second target. Add that same cavity to the
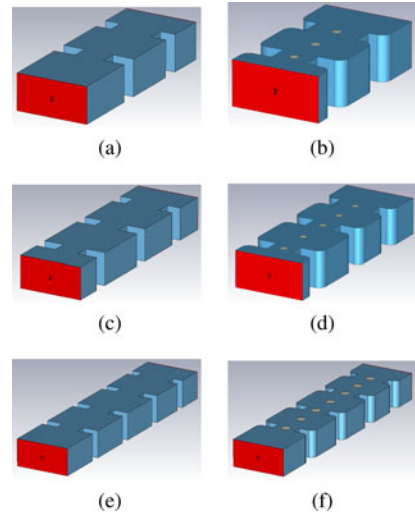

Fig. 2. Filter models used in the first stage of the Efficient ASM: (a) coarse model; (b) fine model. Filter models used in the second stage: (c) coarse model; (d) fine model. Filter models used in the third stage: (e) coarse model; (f) fine model.

fine model (including rounded corners and all tuners, as shown in Fig. 2(d)). We now perform another set of ASM iterations with the reduced coarse model shown in Fig. 2(c). It is important to note that, since the first three elements of the filter have already been obtained, we only need to optimize the newly added parameters (the length of the second cavity, and the width of the output aperture). For some filters, a final optimization of all five parameters may be required to obtain a very good final agreement with the target response, however, this is not the case for our inductive filter.

(v) This procedure is repeated until we reach the center of the filter (see Fig. 2(f)).

(vi) We now obtained a very good starting point for all the dimensions of our filter since the structure is symmetric (Fig. 1 top). At this point, we will perform a final OS-ASM optimization using all design parameters to obtain the desired final performance. This step is normally very fast, since the response of the filter is already very close to the target performance.

Table 2 shows the evolution of the design parameters in the Efficient ASM process. As it can be seen, only two or three

Table 2. Evolution of the design parameters for the inductive six-pole filter in the Efficient ASM process. The design variables are the widths of the apertures (their thickness is fixed to 3.5 mm) and the lengths of the resonators (their heights and widths are set to 9.525 and 19.95 mm). All dimensions are in mm

	Coarse	Fine				
Parameter	Optimum	Iter. 0	Iter. 1	Iter. 2	Iter. 3	Iter. 4
i_1	12.1369	12.1369	11.9096	11.9096	11.9096	11.9226
l_1	13.8491	13.8491	13.4777	13.4777	13.4777	13.4883
i_2	9.0745	9.0745	8.9043	8.9043	8.9043	8.8863
l_2	16.2220	–	16.2220	15.8688	15.8688	15.8929
i_3	8.3179	–	8.3179	8.1321	8.1321	8.1316
l_3	16.6566	–	–	16.6566	16.3198	16.3202
i_4	8.1931	–	–	8.1931	8.0245	8.008
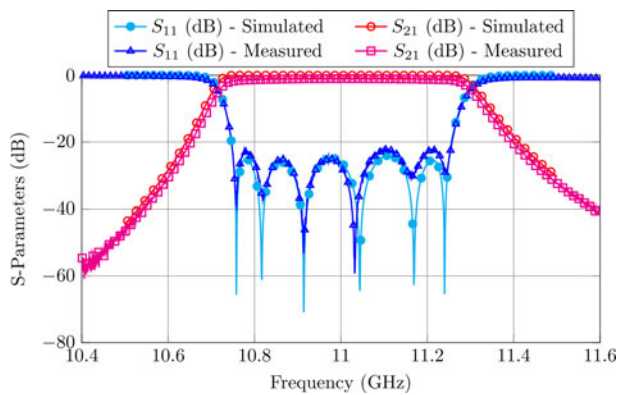
Fig. 3. Measured and simulated response of the six-pole inductive filter.

Fig. 4. Top: Coarse model of the five-pole filter with sharp corners, and without tuning elements (Fig. 1 from [22]). Bottom and center: Fine model of the filter with rounded corners and tuning elements (Fig. 26 from [22]).

variables are optimized in each step. Once we have designed half of the filter, we can duplicate it obtaining a very good performance. The last ASM iteration (which considers all design variables) is very fast, since all elements are very close to their target. Figure 3 shows the performance of the final fine model compared to the measurements of the hardware. As we can see, the agreement is indeed excellent. The Efficient ASM just described is 1.83 times faster than OS-ASM described in the previous section [12] (see Table 3 for the details).

Dual-mode filter

The second application example that we discuss is a more complex five-pole dual-mode filter [22]. The dual mode resonator exploits the resonance of a metallic post, together with the resonance of the rectangular cavity that contains the post. The filter is
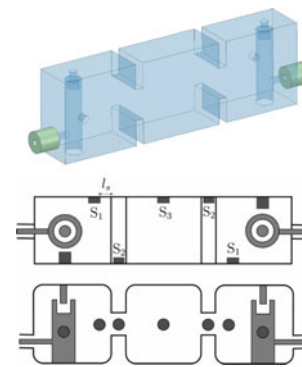
centered at 10 GHz, and has a bandwidth of 300 MHz. Figure 4 (top) shows the *ideal* coarse model of the filter.

As already mentioned, there are two modes resonating in both the first and last cavities. The two resonances are the second resonance of the (re-entrant) post and the first resonance of the rectangular metallic enclosure. The dimensions of both the post and the metallic enclosure are chosen so that the two resonances occur at the same frequency (degenerate modes). The filter will again be manufactured using milling. The fine model must, therefore, include rounded corners (2 mm radius). In addition, it must also include tuning elements (0.9 mm radius) set at a fixed depth of 1 mm. Figure 4 (bottom) shows the fine model of the filter. The design parameters are the lengths of the cavities, the widths of the inductive irises (their thickness is fixed at 2 mm), together with the additional design variables shown in Fig. 5,

Table 3. Performance of both design methods for the in-line six-pole inductive waveguide filter

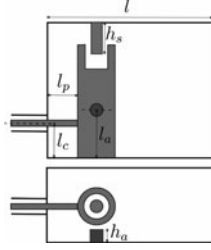| OS-ASM		Efficient ASM					
TC	0.23 s.	TC_1	0.1 s.	TF_1	19 s.	l_1	56
TF	61 s.	TC_2	0.11 s.	TF_2	33 s.	l_2	71
NI	4	TC_3	0.13 s.	TF_3	41 s.	l_3	78
AI	424	TC_4	0.26 s.	TF_4	61 s.	l_4	212
Total	**11 min. 35 s.**	**Total**	**6 min. 20 s.**				

Fig. 5. Dimensions that are optimized in the design process (Fig. 15 from [22]).

Fig. 6. Fine model of the filter that includes tuning elements.
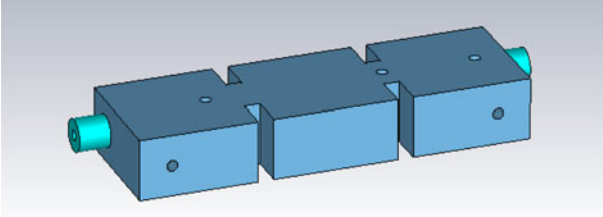

Fig. 7. ASM process to recover the desired performance of the fine model that includes tuning elements.

namely, the height of the re-entrant post (h_s), the height and offset of the cylinder that couples the two degenerate modes (h_a and l_a), the offset of the input/output coaxial port of the filter (l_c), and the length of the connection from the coaxial port to the post (l_p).

The coarse model is again simulated with FEST3D. However, in order to simulate the re-entrant post, FEST3D uses a module based on the well-known 3D Boundary Integral-Resonant Mode Expansion (BI-RME) method [23]. As a result, the simulation is not as fast as the one of the inductive filter we discussed in the previous section. The high precision model is simulated, in this case, using CST. In order to achieve numerical convergence, we increased the density of CST's default initial mesh and let the adaptive mesh perform 24 iterations (using around 1 500 000 tetrahedrons).

OS-ASM
The first step in the design process is to obtain the dimensions of the coarse model (low accuracy) in Fig. 4 (top) that produces the desired response. This can be done, for instance, following the approach described in [21]. Due to the complexity of the hardware, however, it is more convenient to start directly with a two-pole rather than with a one-pole structure. Once the low accuracy two-pole structure is optimized, the complete filter can be assembled, and the central cavity optimized to get the desired response. A global optimization is also necessary to obtain a perfectly compliant set of dimensions for the coarse model.

Once the coarse model has been fully defined, we can start the OS-ASM design of the fine model. In this case, however, it is more convenient to proceed in two stages: in the first one we consider the tuning elements, and in the second one we add the rounded corners. The complete procedure is as follows:

(i) Add first the tuning elements to the fine model (see Fig. 6) using, at the start of the procedure, the structural dimension of the coarse model. After three ASM iterations, both models provide a very similar response (see Fig. 7). It is important to note that, if we had included at this stage also the rounded corners, the initial performance of the fine model would have been too different from the target, and the coarse
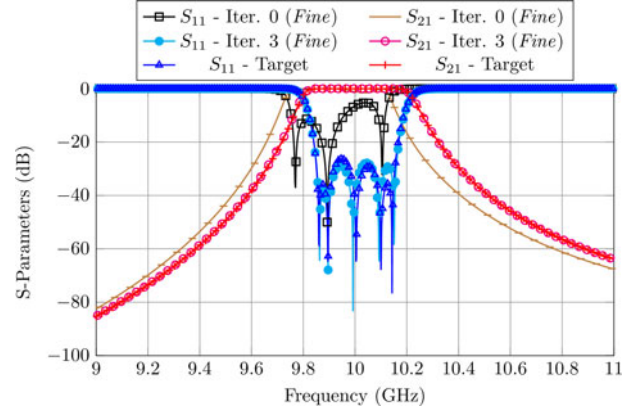
model would have required a significantly longer time to recover the performance of the fine model.

(ii) We can now add the rounded corners to the fine model, obtaining the structure shown in Fig. 4 (bottom). After three more ASM iterations, the fine model gives the desired target response (see Fig. 8).

The overall time required to design the five-pole dual-mode filter using this approach can be computed as:

$$\text{Time} = \sum_{i=1}^{\text{Stages}} TC_i \cdot AI_i \cdot NI_i + (NI_i + 1) \cdot TF_i \qquad (5)$$

$$\text{Time} = 19\,\text{h}\,22\,\text{min}\,28\text{s} \qquad (6)$$

where TC_i and TF_i are the computation times of the coarse and fine models, NI_i is the number of ASM iterations performed, and AI_i is the average number of simulations it takes a simplex algorithm to recover each of the fine model responses.

Efficient ASM
In this case, the segmentation of the problem into smaller optimization spaces is more challenging. This is because the first cavity includes already six out of the total eight design variables. And, furthermore, the six variables are not completely independent. However, the segmentation strategy can still increase significantly the efficiency of the design process with respect to the one described in the previous section. The proposed approach is as follows:

(i) The first step is again to generate a coarse model of the complete first cavity, including the coaxial input, the first cavity (with all its elements) and the first iris (see Fig. 9 left). This model can be rapidly optimized to obtain the desired two-pole performance.

(ii) The next step is to build the fine model of the first cavity including all tuning elements and rounded corners (see Fig. 9 right).

(iii) We can now use the OS-ASM method to align the coarse and the fine models. After two ASM iterations, both models provide the same performance (see Fig. 10). It is important
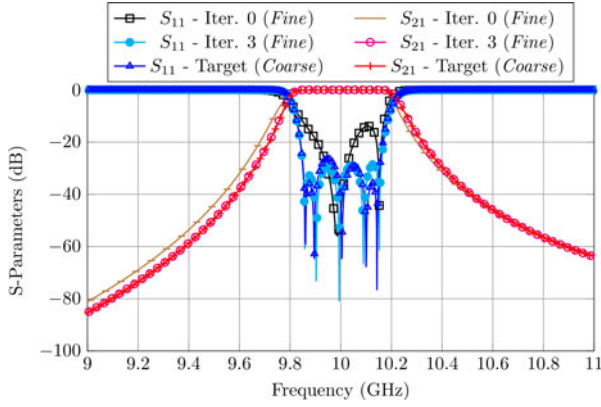
Fig. 8. ASM process to recover the desired performance in the fine model including both tuning elements and rounded corners.
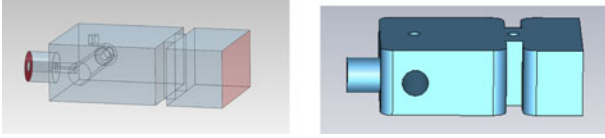

Fig. 9. First reduced model of the filter. Left: coarse model. Right: fine model.
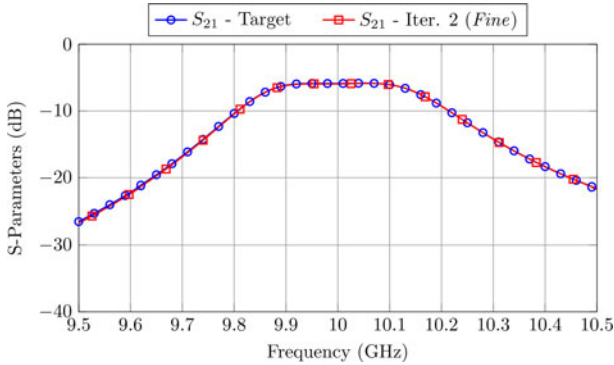

Fig. 10. ASM process to recover the desired performance in the first reduced fine model.

Fig. 11. Top: Second coarse models of the filter. Bottom: Second fine model of the filter.
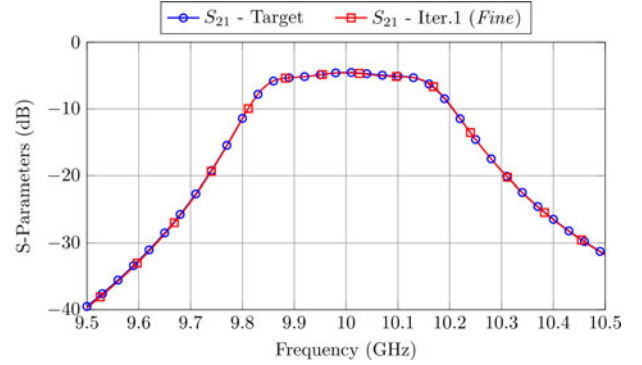
Fig. 12. ASM process to recover the desired performance in the second reduced fine model.

to note that, even if we are optimizing seven parameters (all the dimensions from Fig. 9), the reduced coarse model is twice as fast as the coarse model of the complete filter.

(iv) We then add the central cavity to the coarse model and optimize the structure to obtain the required three-pole performance.

(v) Add next the central resonator and iris to the fine model, obtaining the second fine model shown in Fig. 11 (bottom). Perform one ASM iteration optimizing, primarily but not exclusively, the newly added elements. Figure 12 shows the performances of the fine and coarse models after the ASM process.

(vi) Finally, duplicate the first dual-mode cavity of the fine model to obtain the complete structure of the filter (Fig. 4, bottom). After only one ASM iteration with all the design parameters, the high precision model gives the desired performance (see Fig. 13).
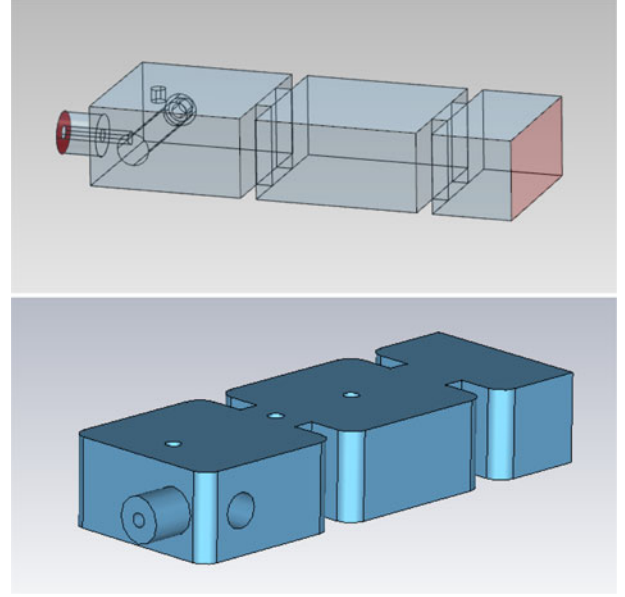
The overall time required to design the five-pole band-pass filter is computed as:

$$\text{Time} = \sum_{i=1}^{\text{Stages}} TC_i \cdot AI_i \cdot NI_i + (NI_i + 1) \cdot TF_i \tag{7}$$

$$\text{Time} = 3\,\text{h}\,37\,\text{min}\,58\text{s} \tag{8}$$

This is 5.3 times faster than the method described in the previous section. Table 4 shows the time parameters of each procedure. It is therefore clear that, using the step-by-step approach based on partial models of the filter can always reduce very significantly the overall time required to obtain the desired target performance with the fine model. Table 5 shows the optimal dimensions for the coarse and fine models.

Tuning techniques

Having successfully designed high precision models of our filters, we now need to move to the next phase, namely, tuning the filters
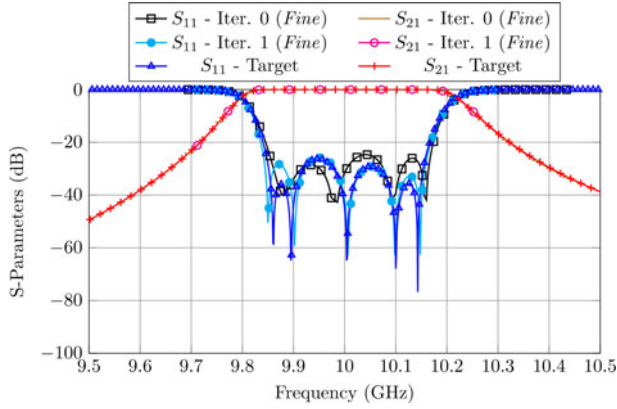
Fig. 13. Final performance of the fine model compared to its target.

Table 5. Optimum dimensions for the design variables of the coarse and fine models of Fig. 4. All dimensions are in mm. Figure 5 shows a drawing with the meaning of the variables. w_{iris} and l_{cavity_2} are, respectively, the width and length of the inductive iris and central cavity

Parameter	Coarse	Fine
w_{iris}	6434FC 7.663	8.092
h_a	6434FC 1.6	1.697
h_s	6434FC 2.547	2.815
l	6434FC 19.143	18.821
l_a	6434FC 9.75	9.956
l_c	6434FC 4.771	4.801
l_{cavity_2}	6434FC 20.396	19.798
l_p	6434FC 3.5011	3.3236

after they have been manufactured. In this context, we first discuss a robotic tuner that we have developed to facilitate the tuning process. We then discuss two different tuning procedures: an ASM-based technique, and another approach that is based on available tuning knowledge.

Tuning robot

One issue that is important to note is that, in order to tune a filter, we must be able to control very precisely the motion and the position of all tuning elements. To do that, in a controllable and systematic way, we have built a simple precision robotic tuner, as shown in Fig. 14. The robotic tuner has three parts: a movable X-Y table to which the filter is fastened, a precision rotating arm with an actuator that can be coupled to the tuning elements, and three drivers connected to a PC to control the tuning process. The rotating arm is driven by a stepper motor with 800 steps for revolution. In addition, there is a 1:30 reduction gear. The resulting theoretical (minimal) uncertainty is 0.015 degrees. However, we have observed that, in practice, the angular accuracy of the system is about one degree. Taking into account that the pitch of the tuning elements is 0.397 mm, this results in a penetration accuracy of about one μm. This is enough to tune a large variety of filters.

ASM-based tuning procedure

The first tuning procedure is based on ASM [19]. As usual, this technique uses two simulation models: the fine model shown in
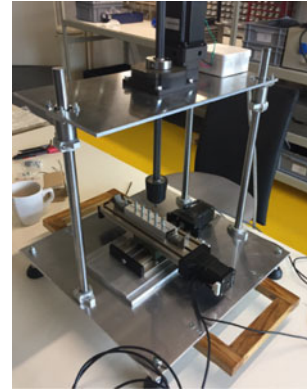

Fig. 14. Precision robotic tuner that we have built to control the tuning process.

the top of Fig. 1, and the coarse model shown in the bottom of Fig. 1, respectively. The starting point of the tuning procedure is, in fact, what we know at the end of the filter design process, namely, that both the coarse and the fine model are *aligned* with the desired performance (Fig. 15). Furthermore, in the vicinity of the alignment point, we know that relation between the two models (or spaces) is given by (1), where it is important to recall that:

• $\mathbf{x_f}$ refers to the penetrations of the tuners in the fine model shown in Fig. 1 (top).

Table 4. Performance of both design methods for the five-pole filter based on dual-mode coaxial resonators

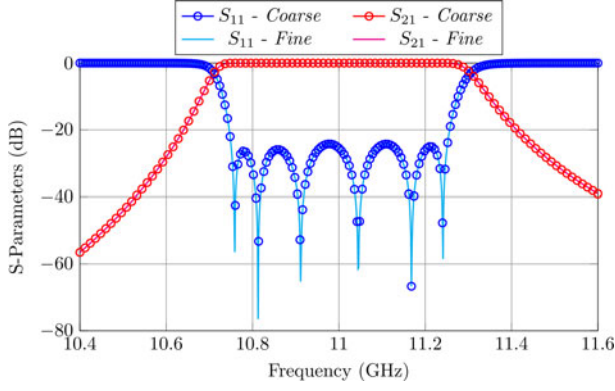| One-step ASM							
TC_1	15.74 s	TF_1	371 s	AI_1	729	NI_1	3
TC_2	15.74 s	TF_2	386 s	AI_1	684	NI_1	3
Total	**19 h 22 min 28 s**						
Efficient ASM							
TC_1	8.07 s	TF_1	123 s	AI_1	251	NI_1	2
TC_2	8.23 s	TF_2	176 s	AI_2	204	NI_2	1
TC_3	15.74 s	TF_3	386 s	AI_3	372	NI_3	1
Total	**3 h 37 min 58 s**						

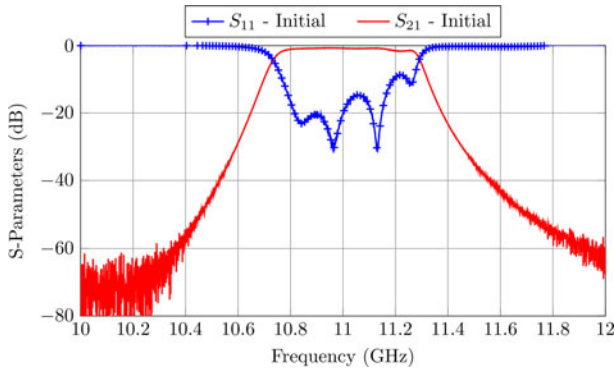**Fig. 15.** Aligned performances of the coarse and fine models of the inductive filter.

Fig. 16. Performance of the filter when all tuning elements are set to the design depth.

- x_c refers to the waveguide dimensions of the coarse model shown in Fig. 1 (bottom).

To proceed, we now need to compute the **B** matrix in (1). To do that, we now modify, one at the time, the penetration of each tuner of the fine model (indicated by x_{fi}) and optimize instances of the coarse model to recover the fine model performances (x_{ci}). After doing that, following the procedure detailed in [20], we can easily compute the elements of the matrix **B** that relates the filter dimensions of the coarse model with the penetrations of the tuning elements. Now that we have a good estimation of the **B** matrix at the point of alignment, we can proceed with the tuning process, as follows:

(i) Once the filter is manufactured, set the tuners at their design penetration (given by x_1). This will provide, in our case, the response shown in Fig. 16, which we will refer to as $R_m(x_1)$.

(ii) Optimize an instance of the coarse model until we recover the same performance, namely:

$$R_c(x_{cm}) = R_m(x_1) \qquad (9)$$

(iii) Set the tuners of the filter to:

$$x_2 = x_1 + \mathbf{B} \cdot (x_{copt} - x_{cm}) \qquad (10)$$

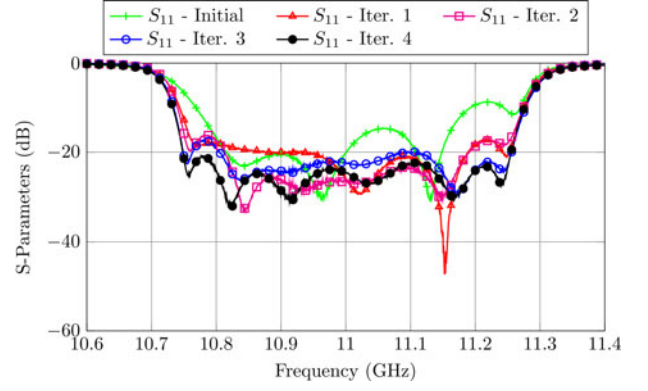(iv) Go back to step (i) and repeat this process until the filter is completely tuned.

Fig. 17. Filter performance after every ASM iteration.

After four ASM iterations, our filter is successfully tuned as shown in Fig. 17.

A knowledge-based approach

The ASM-based technique we just discussed could also be used for tuning the dual-mode filter. However, due to the relatively long simulation time that is required in this case (about 15 s for a single run), and the expected number of coarse simulations in each ASM iteration (about 600–700), the use of the ASM-based tuning technique would require a total of about 10–11 h.

We therefore propose to apply a different knowledge-based tuning approach. Our objective has been, in fact, to develop a semi-automatic tuning approach that is based on the manual tuning procedure that is widely used in the industrial environment. A key step in this context is to use Matlab to *read* the measurements of a VNA so that they can be further processed to support the tuning process. The resulting procedure is then as follows:

(i) Define first the S11 and S21 tuning masks. In this case, the return loss between 9.85 and 10.15 GHz should be lower than −30 dB, and the S21 at 9.6 and 10.53 GHz should have minimum attenuation level of −40 dB. The S11 error at each point is then computed using the following expression:

$$e_{s_{11}}{}^{(i)} = \begin{cases} RL_{goal} - RL^{(i)}, & \text{if } RL^{(i)} < RL_{goal} \\ 0, & \text{otherwise} \end{cases} \qquad (11)$$

and the S21 error is defined as:

$$e_{s_{21}}{}^{(i)} = \begin{cases} IL_{goal} - IL^{(i)}, & \text{if } IL^{(i)} < IL_{goal} \\ 0, & \text{otherwise} \end{cases} \qquad (12)$$

The total error is then computed as:

$$E = \frac{w_1}{n_1} \sum_{i=1}^{n_1} e_{s_{11}}{}^{(i)} + \frac{w_2}{n_2} \sum_{i=1}^{n_2} e_{s_{21}}{}^{(i)}, \qquad (13)$$

where w_1 and w_2 are the weights for the S11 and S21 terms, and n_1 and n_2 are the number of points used in each mask.

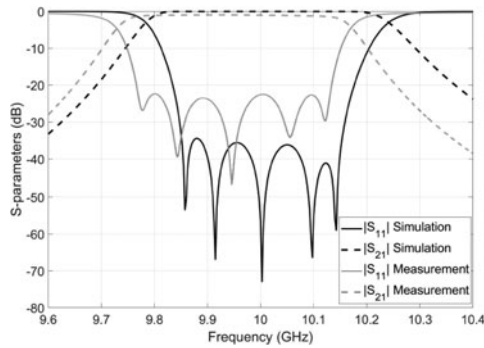(ii) The next step is to set all tuners to the design penetration.

Fig. 18. Final performance of the filter after the tuning process.

(iii) We can then start the actual tuning procedure that consists of finding the penetration of each tuning element that minimizes the total error that we have just defined. A key step is now to define the order in which the tuners must be modified.

(iv) Following the guidelines from [24], we will first act upon the tuners in the cavities and then we will adjust the tuners that control the couplings. After each tuner movement, the error is recomputed using Matlab to decide if the movement must be kept or discarded (i.e., to return to the original position).

(v) This process is repeated until the filter is tuned, and all masks are satisfied.

Figure 18 shows the performance of the filter at the end of the tuning process. As we can see, the performance that we have obtained is good but is not in perfect agreement with the simulations. Further investigations indicated that this disagreement is due to the dimensional errors introduced by the manufacturing process, in particular, with respect to the input and output couplings [22]. Our tuning procedure, however, was able to obtain, with a very reasonable effort, the best possible performance that the hardware could give. Finally, it is important to note that the successful use of the procedure just described does not require any previous tuning experience.

Conclusions

To reduce the costs of microwave filters, it is common practice to use a manufacturing technique that can deliver an intermediate (low cost) accuracy, like milling for instance, together with tuning elements that can be adjusted after manufacturing in order to obtain the desired filter performance. An inevitable consequence of this choice is that the presence of rounded corners and tuning elements must be included in the design process. This, in turn, can result in a significantly increased EM simulation effort. In this context, therefore, we have discussed in this paper two efficient design strategies that can be used to significantly decrease the computational effort to design microwave filters commonly used for both ground and space applications. In addition to filter design strategies, we have also discussed two systematic procedures to support the filter tuning stage.

The value of this contribution is, in our opinion, that the material discussed can, in fact, be considered as an end-to-end guide enabling young engineers to deliver compliant microwave filter designs with a minimum of previous experience.

References

1. **Strategic Research Agenda, European Space Technology Platform.**
2. **Snyder RV** (2007) Practical aspects of microwave filter development. *IEEE Microwave Magazine*, **8**, 42–54.
3. **Bandler JW, Biernacki RM, Chen SH, Grobelny PA and Hemmers RH** (1994) Space mapping technique for electromagnetic optimization. *IEEE Transactions on Microwave Theory and Techniques*, **42**, 2536–2544.
4. **Bandler JW, Biernacki RM, Chen SH, Hemmers RH and Madsen K** (1995) Aggressive space mapping for electromagnetic design. *IEEE MTT-S International Microwave Symposium, May*, Orlando, FL, USA, IEEE, pp. 1455–1458.
5. **Bandler JW, Biernacki RM, Chen SH, Hemmers RH and Madsen K** (1995) Electromagnetic optimization exploiting aggressive space mapping. *IEEE Transactions on Microwave Theory and Techniques*, **43**, 2874–2882.
6. **Diaz Caballero E, Morro J, Belenguer A, Esteban H and Boria V** (2013) CAD technique for designing H-plane waveguide filters considering rounded corners. *IEEE MTT-S International Microwave Symposium Digest*, Seattle, WA, USA, IEEE, pp. 1–3.
7. **Ismail MA, Smith D, Panariello A, Wang Y and Yu M** (2003) EM based design of large-scale dielectric resonator multiplexers by space mapping. *IEEE MTT-S International Microwave Symposium Digest*, Philadelphia, PA, USA, IEEE, pp. 291–294.
8. **Brumos M, Boria VE, Guglielmi M and Cogollos S** (2014) Correction of manufacturing deviations in circular-waveguide dual-mode filters using aggressive space mapping. *44th European Microwave Conference*, pp. 624–627, EuMA, Rome, Italy.
9. **Rayas-Sanchez JE** (2016) Power in simplicity with ASM: tracing the aggressive space mapping algorithm over two decades of development and engineering applications. *IEEE Microwave Magazine*, **17**, 64–76.
10. **Ossorio J, Vague J, Boria VE and Guglielmi M** (2017) Efficient implementation of the aggressive space mapping technique for microwave filter design. *47th European Microwave Conference*, Nuremberg, Germany, EuMA, pp. 644–647.
11. **Ossorio J, Melgarejo JC, Boria VE, Guglielmi M and Bandler JW** (2018) On the alignment of low-fidelity and high- fidelity simulation spaces for the design of microwave waveguide filters. *IEEE Transactions on Microwave Theory and Techniques*, **66**, 5183–5196.
12. **Melgarejo JC, Guglielmi M, Cogollos S and Boria VE** (2021) An efficient microwave filter design procedure based on space mapping. *2020 50th European Microwave Conference*, Jaarbeurs Utrecht, The Netherlands, EuMA, pp. 743–746.
13. **Koziel S, Cheng QS and Zhang Q** (2016) On low-cost space mapping optimization of antenna structures. *2016 IEEE MTT-S International Conference on Numerical Electromagnetic and Multiphysics Modeling and Optimization*, San Francisco, CA, USA, IEEE, pp. 1–2.
14. **Cheng QS, Bandler JW and Koziel S** (2015) A review of implicit space mapping optimization and modeling techniques. *2015 IEEE MTT-S International Conference on Numerical Electromagnetic and Multiphysics Modeling and Optimization*, Phoenix, AZ, USA, IEEE, pp. 1–3.
15. **Koziel S** (2017) Space mapping: performance, reliability, open problems and perspectives. *2017 IEEE MTT-S International Microwave Symposium Digest*, Honolulu, HI, USA, IEEE, pp. 1512–1514.
16. **Miraftab V and Mansour RR** (2006) Automated microwave filter tuning by extracting human experience in terms of linguistic rules using fuzzy controllers. *IEEE MTT-S International Microwave Symposium Digest*, San Francisco, CA, USA, IEEE, pp. 1439–1442.
17. **Mirzai AR, Cowan CFN and Crawford TM** (1989) Intelligent alignment of waveguide filters using a machine learning approach. *IEEE Transactions on Microwave Theory and Techniques*, **37**, 166–173.
18. **Zhou J and Huang J** (2013) Intelligent tuning for microwave filters based on multi-kernel machine learning model. *5th IEEE International Symposium on Microwave, Antenna, Propagation and EMC Technologies for Wireless Communications*, Chengdu, China, IEEE, pp. 259–266.

19. **Melgarejo JC, Guglielmi M, Cogollos S and Boria VE** (2019) Space mapping for tuning microwave waveguide filters. *IEEE MTT-S International Microwave Symposium (IMS),* Boston, MA, IEEE, pp. 353–356.

20. **Melgarejo JC, Ossorio J, Cogollos S, Guglielmi M, Boria VE and Bandler JW** (2019) On space mapping techniques for microwave filter tuning. *IEEE Transactions on Microwave Theory and Techniques*, **67**, 4860–4870.

21. **Guglielmi M and Melcon AA** (1993) Novel design procedure for microwave filters. *1993 23rd European Microwave Conference, September*, Madrid, Spain, EuMA, pp. 212–213.

22. **San-Blas ÁA, Guglielmi M, Melgarejo JC, Coves Á and Boria VE** (2020) Design procedure for bandpass filters based on integrated coaxial and rectangular waveguide resonators. *IEEE Transactions on Microwave Theory and Techniques*, **68**, 4390–4404.

23. **Arcioni P, Bozzi M, Bressan M, Conciauro G and Perregrini L** (2002) Frequency/time-domain modeling of 3D waveguide structures by a BI-RME approach. *International Journal of Numerical Modelling*, **15**, 3–21.

24. **Lindner A and Biebl E** (2006) A manual tuning method for coupled cavity filters. *36th European Microwave Conference*, Manchester, UK, EuMA, pp. 1340–1342.